1-31-2023

Atomistic Details of Peptide Reversed-Phase Liquid Chromatography from Molecular Dynamics Simulations

Pablo M Scrosati

Lars Konermann
konermann, konerman@uwo.ca

Atomistic Details of Peptide Reversed-Phase Liquid Chromatography from Molecular Dynamics Simulations

Pablo M. Scrosati and Lars Konermann*

Department of Chemistry, The University of Western Ontario, London, Ontario, N6A 5B7, Canada

* To whom correspondence should be addressed. E-mail: konerman@uwo.ca.

ABSTRACT: Peptide separations by reversed-phase liquid chromatography (RPLC) are an integral part of bottom-up proteomics. These separations typically employ C18 columns with water/acetonitrile gradient elution in the presence of formic acid. Despite the widespread use of such workflows, the exact nature of peptide interactions with the stationary and mobile phases are poorly understood. Here we employ microsecond molecular dynamics (MD) simulations to uncover details of peptide RPLC. We examined two tryptic peptides, a hydrophobic and a hydrophilic species, in a slit pore lined with C18 chains that were grafted onto SiO_2 support. Our simulations explored peptide trapping, followed by desorption and elution. Trapping in an aqueous mobile phase was initiated by C18 contacts with Lys butyl moieties. This was followed by extensive anchoring of nonpolar side chains (Leu/Ile/Val) in the C18 layer. Exposure to water/acetonitrile triggered peptide desorption in a stepwise fashion; charged sites close to the termini were the first to lift off, followed by the other residues. During water/acetonitrile elution, both peptides preferentially resided close to the pore center. The hydrophilic peptide exhibited no contacts with the stationary phase under these conditions. In contrast, the hydrophobic species underwent multiple transient Leu/Ile/Val binding interactions with C18 chains. These nonpolar interactions represent the foundation of differential peptide retention, in agreement with the experimental elution behavior of the two peptides. Extensive peptide/formate ion pairing was observed in water/acetonitrile, particularly at N-terminal sites. Overall, this work uncovers an unprecedented level of RPLC molecular details, paving the way for MD simulations as a future tool for improving retention prediction algorithms, and for the design of novel column materials.

Introduction

Reversed-phase liquid chromatography (RPLC) is one of the most widely used analytical tools in biochemical research, drug development, environmental testing, food chemistry, clinical analyses, forensics, and many other areas.[1-5] Typical RPLC columns contain a stationary phase consisting of porous silica (SiO_2) particles that carry surface-bound alkyl chains, often C4, C8, or C18 moieties.[3-6] The mobile phase being pumped through the column is a mixture of water and an organic cosolvent such as acetonitrile.[2, 3] This mobile phase is acidified, e.g., by formic or trifluoroacetic acid, generating conjugate base anions that can act as ion pairing agents.[7-12]

Separation in RPLC is based largely on hydrophobic contacts between the analyte and the stationary phase.[2, 13] Simply speaking, analytes that bind strongly to the stationary phase elute later, because binding restricts their convective transport in the mobile phase.[14] In reality, the situation is more complex, because RPLC separations employ gradient elution where the mobile phase composition changes over time.[13] The process starts with a high-water percentage to promote analyte trapping on the stationary phase close to the column inlet.[13] The organic content is then gradually ramped up, such that analytes desorb and migrate through the column. Nonpolar analytes migrate more slowly, because they experience more extensive interactions with the stationary phase. Ideally, this process results in well separated chromatographic bands.[15] The molecular mechanism of analyte retention has been a subject of debate for many years, particularly the question whether analytes adsorb on, or partition into, the stationary phase. Today it is believed that both factors can contribute, as governed by the properties of the stationary and mobile phases, as well as the nature of the analyte.[16-20]

Electrospray ionization (ESI) mass spectrometry (MS) represents one of the most versatile detection methods for RPLC. Analytes that elute off the column are converted into gaseous ions

by the ESI source. These ions are then analyzed by the mass spectrometer. Conveniently, typical RPLC mobile phases are "ESI-friendly", providing high signal stability and intensity,[21, 22] particularly when using formic acid (trifluoroacetic acid suppresses ESI-MS signals).[1, 8, 12, 23]

RPLC/ESI-MS is particularly important for proteomics. Most bottom-up workflows involve the analysis of peptides generated using trypsin, a protease that cleaves on the C-terminal side after Arg and Lys (unless followed by Pro).[24-26] Similar RPLC-based bottom-up strategies are used for protein hydrogen/deuterium exchange,[27] covalent labeling,[28, 29] and crosslinking.[30, 31] Peptide separation in bottom-up experiments is typically performed on C18 columns with a water/acetonitrile LC gradient in the presence of 0.1% formic acid.[1, 3, 5, 12, 25, 27, 32] Under these low pH conditions, acidic groups (Asp and Glu side chains, C-termini) are neutral, while basic sites (Arg, Lys, His, N-termini) are positively charged.[33]

The optimization of RPLC separations often involves labor-intensive trial-and-error procedures aimed at identifying the best gradient, column material, temperature, pH, ion pairing agent, etc.[34-36] Retention prediction algorithms can help streamline these optimization efforts, and they can assist in analyte identification by providing information that is complementary to analyte mass and MS/MS fragments.[15, 37-41] Current retention prediction algorithms employ semi-empirical modelling and machine learning.[15, 41] Much remains to be learned about the exact relationships that govern the interplay between analyte composition, conformation, and interactions with the stationary and mobile phases A better mechanistic understanding of analyte retention could streamline RPLC method optimization, improve the robustness of prediction algorithms, and aid in the development of novel column materials.

Computational techniques can provide atomistic insights into a wide range of (bio)chemical processes. For example, Monte Carlo (MC) simulations report on the equilibrium

behavior of various solute/solvent systems, while molecular dynamics (MD) simulations can uncover both equilibrium and kinetic aspects. These computational tools have led to major advances in various fields.[42-44] Surprisingly, the application of computer simulations to RPLC remain limited, despite the tremendous promise of this approach.[41, 45, 46] Some MD and MC studies examined RP stationary phases in various solvents.[47-52] Others focused on stationary phase interactions with short alkanes[19, 53, 54] and benzene derivatives.[55, 56] Computational studies of peptide RPLC are more challenging, owing to the relatively large size of these analytes, their conformational dynamics, and their chemical diversity. Consequently, only few computational forays into peptide RPLC have been undertaken. Those studies employed very short simulation time windows (tens of ns or less),[57, 58] leaving major gaps in the mechanistic understanding of proteomic workflows.

The current study uses microsecond MD simulations to uncover novel information on peptide RPLC mechanisms by probing how tryptic digestion products with different sequences interact with a C18 stationary phase. Rather than attempting to provide retention predictions for a large number of peptides, we focused on two model species with different physicochemical properties to examine fundamental aspects. All three stages of the RPLC process were investigated, i.e., peptide trapping in an aqueous mobile phase, as well as desorption, and elution in water/acetonitrile. The data obtained in this way provide the most detailed insights to date into the atomistic foundation of peptide RPLC.

Materials and Methods

Myoglobin (Mb) was purchased from Sigma (St. Louis, MO). Sequencing grade trypsin was from Promega (Madison, WI). Peptides were separated on a Waters (Milford, MA) BEH C18 RPLC column with a nanoACQUITY LC using a linear water/acetonitrile gradient, coupled to a Waters Synapt G2-Si Q-TOF mass spectrometer. GROMACS 2020.4[59] was used for all-atom μs MD simulations with the CHARMM36m forcefield.[60] A stationary phase for MD simulations was assembled using β-cristobalite as support, reflecting the prevalence of this SiO_2 material (or closely related materials) in commercial columns[45, 61] and in previous computational studies.[46, 47] C18 chains [dimethyl octadecyl silane, $-Si(CH_3)_2(C_{18}H_{37})$] were grafted to every second vacant surface oxygen. The remaining vacant oxygens were capped with hydrogen, creating free silanol groups. The resulting C18 and silanol surface densities were 4.7 μmol m^{-2}, matching typical high carbon loading stationary phase properties.[2, 49, 51, 53, 57] Periodic boundary conditions were used to generate a 10 nm wide slit pore, consistent with the pore dimensions of typical porous silica RPLC columns.[5, 62, 63] Similar slit pore geometries have been used in earlier simulations.[45, 46, 54, 64] The number of atoms in our simulations was on the order of 10^5. Simulations were performed on commercially available "gaming" workstations with 4 or 8 core Intel CPUs (Santa Clara, CA), and with NVIDIA GPUs (Santa Clara, CA) that used CUDA acceleration. Wall clock times required for each μs simulation ranged between 10 and 21 days. Additional computational details are provided in Figure S1 and the associated SI text.

Like previous RPLC simulations,[19, 53-56] we did not explicitly model convective transport of analytes in the mobile phase, i.e., the net flow rate was zero. This is justified because average flow velocities in RPLC are on the order of 0.2 nm μs^{-1} for typical conditions with a ~66% column

void volume and a flow rate of 60 μL min^{-1},[65] such that convective analyte displacement is minimal on the time scale of our 1 μs simulations.

Results and Discussion

RPLC Experiments on Tryptic Peptides. Starting point for examining the mechanism of RPLC peptide retention was a bottom-up analysis of the model protein myoglobin. Tryptic digests were separated on a C18 RPLC column using a water/acetonitrile gradient with 0.1% formic acid, followed by on-line ESI-MS. A typical chromatogram is shown in Figure 1A. Peptides T1-T12 eluted as well-separated peaks at different acetonitrile concentrations, and they were identified based on their intact mass and MS/MS fragments (Figure 1B).

For examining peptide-column interactions, this work focused on two peptides. Our aim was to select peptides of similar length, but with different physicochemical properties. We settled on T6 $[Nt^{+}H^{+}GT\mathbf{VVL}TA\mathbf{L}GG\mathbf{IL}K^{+}Ct^{0}]^{3+}$ (retention time 12 min, 37 s) and T7 $[Nt^{+}GH^{+}H^{+}E^{0}AE^{0}\mathbf{L}K^{+}P\mathbf{L}AQSH^{+}ATK^{+}Ct^{0}]^{6+}$ (6 min, 12 s), highlighted in Figure 1 using green and red. These peptides have roughly the same length (14 and 17 residues), such that their retention differences must be related to factors other than size.[66] Bold letters highlight the six highly nonpolar residues (Leu/Ile/Val) in T6, whereas T7 possesses only two of these nonpolar residues. The indicated charges on titratable side chains and termini (Nt and Ct) refer to those encountered in the acidic RPLC mobile phase. The resulting net charge is 3+ and 6+ for T6 and T7, respectively. On the basis of their charge, retention time, and amino acid composition, we will refer to T6 as "hydrophobic peptide", whereas T7 will be denoted as "hydrophilic peptide".

Consistent with our naming convention, T6 and T7 have the highest and the lowest summed Kyte-Doolittle (KD) scores, +16.4 and -18.4 (Figure 1C). KD scores are widely used for characterizing protein sequences,[67] but they are not reliable predictors of RPLC retention (Figure S2).[68] The reason underlying the limited predictive power of KD scores and related parameters such as logP[2, 37, 69, 70] is that they only consider the amino acid composition, but not the peptide sequence, structural dynamics, or ion pairing interactions.[13, 38, 71]

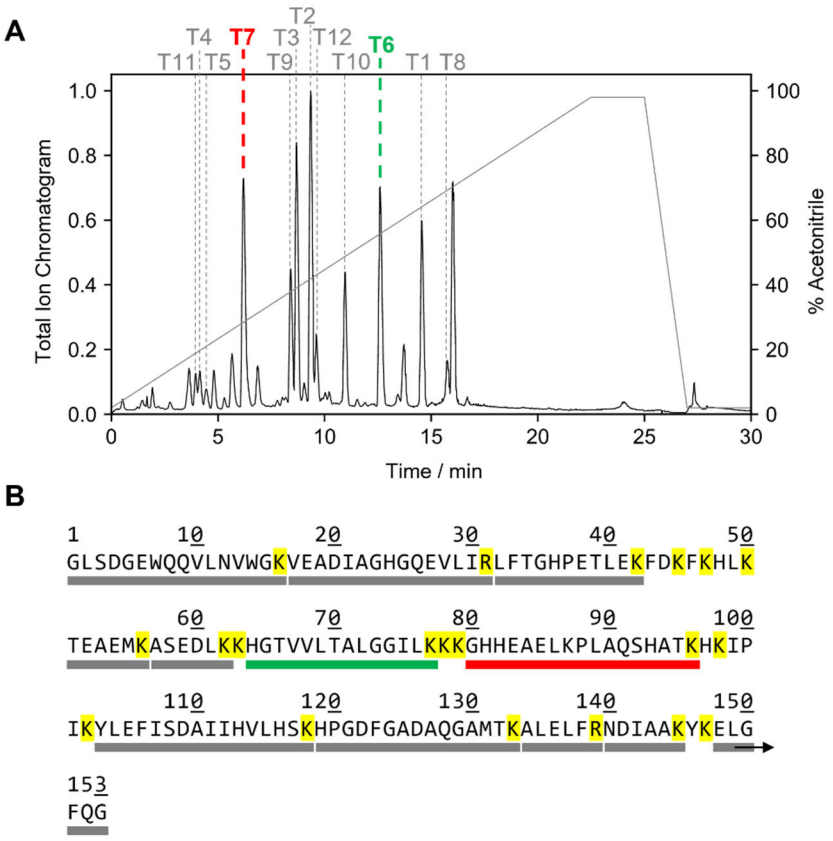

C

	Sequence	Position	KD Score
T1	GLSDGEWQQVLNVWGK	1-16	-9.2
T2	VEADIAGHGQEVLIR	17-31	2.3
T3	LFTGHPETLEK	32-42	-7.1
T4	TEAEMK	51-56	-7.9
T5	ASEDLK	57-62	-6.1
T6	HGTVVLTALGGILK	64-77	16.4
T7	GHHEAELKPLAQSHATK	80-96	-18.4
T8	YLEFISDAIIHVLHSK	103-118	9.7
T9	HPGDFGADAQGAMTK	119-133	-11.0
T10	ALELFR	134-139	4.2
T11	NDIAAK	140-145	-2.8
T12	ELGFQG	148-153	-1.2

Figure 1. RPLC/ESI-MS analysis of myoglobin tryptic peptides. (A) Chromatogram and gradient composition. (B) Myoglobin sequence (PDB 1WLA), with tryptic cleavage sites shown in yellow. Expected peptides > 500 Da are indicated by solid bars below the sequence. (C) Kyte-Doolittle (KD) hydropathy scores of all peptides, calculated by adding the hydropathy values of individual residues.[67] The two peptides examined in subsequent MD simulations are highlighted in green (T6, hydrophobic peptide) and red (T7, hydrophilic peptide).

MD Characterization of Stationary and Mobile Phase. The MD simulations of this work employed a 10 nm wide slit pore built from a C18-grafted silica stationary phase (Figure 2A). Prior to conducting peptide RPLC simulations, we characterized the stationary and mobile phase in the absence of analytes. Two different mobile phases were examined in 500 ns runs, i.e., pure water, and a 1:1 molar mixture of water and acetonitrile. The latter contains 74% acetonitrile by volume. We will refer to this specific mixture as "water/acetonitrile" throughout this manuscript.

In pure water, the solvent was evenly distributed throughout the pore (Figure 2A). The water concentration sharply decreased in the vicinity of the C18 chains, except for local maxima close to the silica surface (Figure 2B). These local maxima arise from buried H_2O molecules that were H-bonded to silanol groups, as seen in earlier RPLC simulations.[55] Water exclusion from most of the C18 layer can be attributed to hydrophobic packing of the alkyl chains. Nonetheless, local parting of the C18 chains occasionally opened up "craters" in the alkyl layer that allowed water protrusions to reach from the bulk all the way to the silica support. Owing to the C18 chain dynamics, these craters were short-lived and persisted only for tens of nanoseconds (Figure S3A).

Filling the pore with water/acetonitrile triggered partial solvent segregation, with a ~1 nm layer at the C18 surface where water was depleted (Figure 2C). The water concentration increased with increasing distance from the C18 chains, having its maximum in the pore center (Figure 2D). Water depletion at the pore walls reflects the fact that alkyl chains interact more favorably with nonpolar molecules (acetonitrile) than with highly polar species (H_2O). Similar segregation at nonpolar surfaces has been reported for other binary solvents.[53-55]

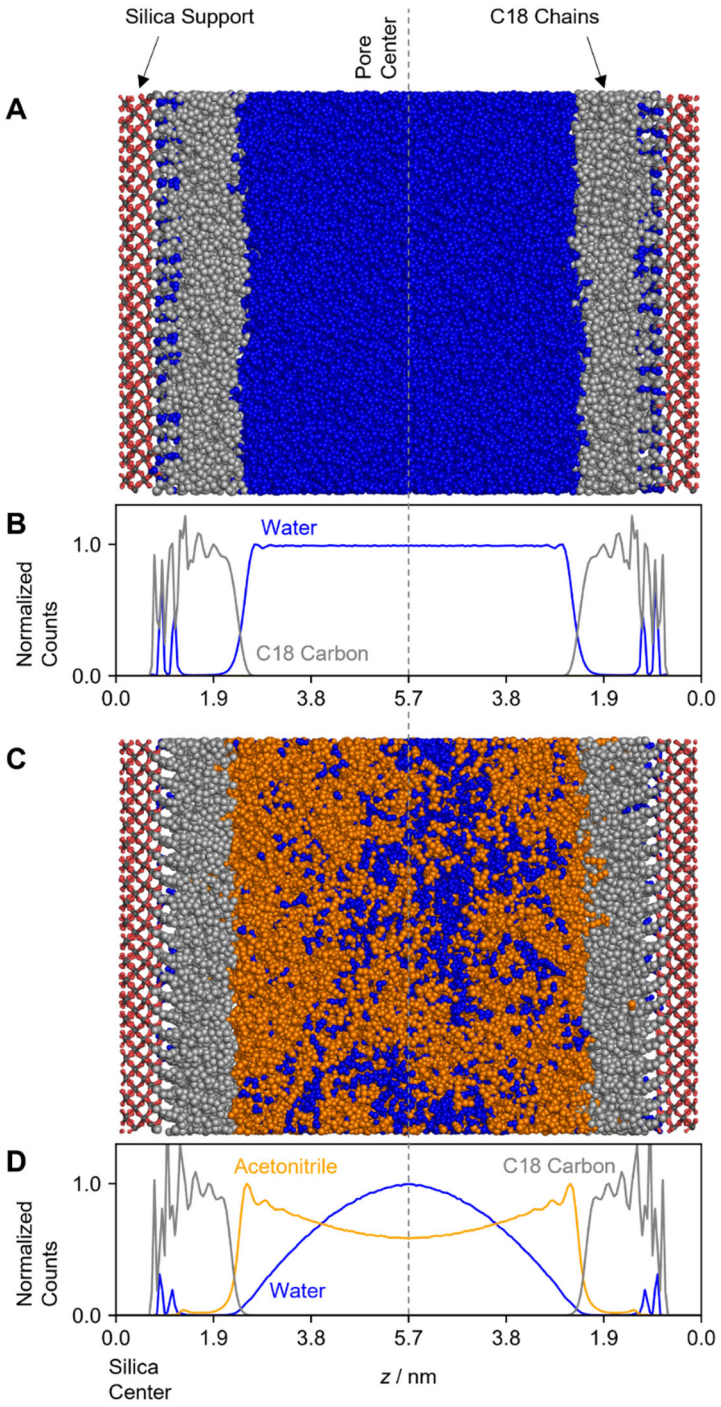

Figure 2. Slit pore used for RPLC simulations, prior to addition of peptides. (A) MD snapshot of a water-filled pore. (B) Molecular distributions for the water-filled pore. (C) MD snapshot of a pore filled with water/acetonitrile. (D) Molecular distributions for the water/acetonitrile-filled pore. C18 chains are shown in light grey, Si and O atoms of the silica support are dark grey and red, respectively. Water molecules are shown in blue, acetonitrile in orange. Panels A and C represent systems at t = 500 ns. Data in panels B and D were averaged over t = 250 to 500 ns.

Inspection of the ~6 nm wide center region of the pore reveals that water/acetonitrile did not form a homogeneous mixture here either (Figure 2C). Instead, acetonitrile was interspersed with a loose network of water clusters, consistent with earlier data on water/acetonitrile[72] and water/alcohol.[73-75] This microimmiscibility is caused by the tendency of H_2O to maximize H-bonding contacts. Each H_2O can form up to four H-bonds with other H_2O molecules,[43] while acetonitrile can only form a single H-bond with H_2O.[72] H-bonding among acetonitrile molecules is not possible. The microimmiscibility seen in the pore center region therefore reflects a compromise between the opposing trends of the solvent to maximize its entropy via mixing, and to minimize its enthalpy via H-bond formation.

Figure 2C/D also shows several water molecules that were buried in the C18 layer and hydrogen-bonded to silanol groups, as well as a few acetonitrile molecules that were interspersed between the alkyl chains. Similar to the water-only simulations, occasional parting of alkyl chains gave rise to short-lived acetonitrile-filled "craters" in the C18 layer (Figure S3B).

Overall, the stationary and mobile phase data of Figure 2 are consistent with expectations and with previous studies, setting the stage for peptide RPLC simulations. The final stationary phase configurations generated for t = 500 ns were used as starting points of these peptide runs.

Peptide Trapping. The first stage of any RPLC separation is analyte trapping on the stationary phase in a mobile phase with high water content.[2, 13] To explore this trapping regime, our initial MD simulations examined peptide interactions with the C18 stationary phase in water. Three independent 1 μs simulations were conducted for both T6 (hydrophobic peptide) and T7 (hydrophilic peptide). For all these runs, a single peptide was initially placed in the pore center, in maximum distance from the C18 chains. Peptide-stationary phase contacts were tracked using (i)

d_{MIN}, i.e., the minimum distance between any peptide atom and any C18 atom, and (ii) d_{COM}, i.e., the distance between the peptide center-of-mass (COM) and the closest Si atom. The information provided by these two metrics is different; $d_{MIN} < 0.25$ nm signifies that at least one amino acid is in direct van der Waals contact with a C18 chain. Conversely, d_{COM} indicates the overall peptide penetration depth into the C18 layer, keeping in mind that this layer is ~2 nm thick (Figure 2B/D).

In all water simulations, the peptides became trapped on the stationary phase within < 1 μs, evident from Figure 3A/B and 3F/G. The time points when d_{COM} dropped to < 2 nm indicate how long it took the peptides to undergo quasi-irreversible binding (Figures 3B/G). These trapping times were shorter for the hydrophobic peptide (between 87 and 291 ns) than for the hydrophilic peptide (177 to 777 ns). Trapping of the hydrophobic peptide took place immediately following its first contact with a C18 chain (Figure 3A/B), whereas the hydrophilic peptide experienced several transient C18 contacts prior to trapping. Such transient contacts are exemplified by the blue trajectory in Figure 3F, where d_{MIN} dipped below 0.25 nm several times prior to trapping at $t = 777$ ns. Despite the variability of the triplicate simulations in Figure 3, the observed binding behavior confirms the expected trend where the hydrophobic peptide has a higher affinity for the C18 chains, promoting faster trapping than for the hydrophilic species.

The MD snapshots of Figure 3 illustrate different stages of peptide trapping. Most of the initial peptide/C18 contacts were mediated by the C-terminal Lys side chains. This behavior may seem surprising, considering that Lys carries a positive charge. However, Lys/C18 contacts only involved the aliphatic region of the $-CH_2-CH_2-CH_2-CH_2-NH_3^+$ side chains, while the charged amino groups remained in water contact (Figure 3C/H). It has been demonstrated previously that Lys can engage in hydrophobic contacts via its aliphatic region, e.g., during protein aggregation.[76] The Lys/C18 contacts seen here are consistent with those earlier data.

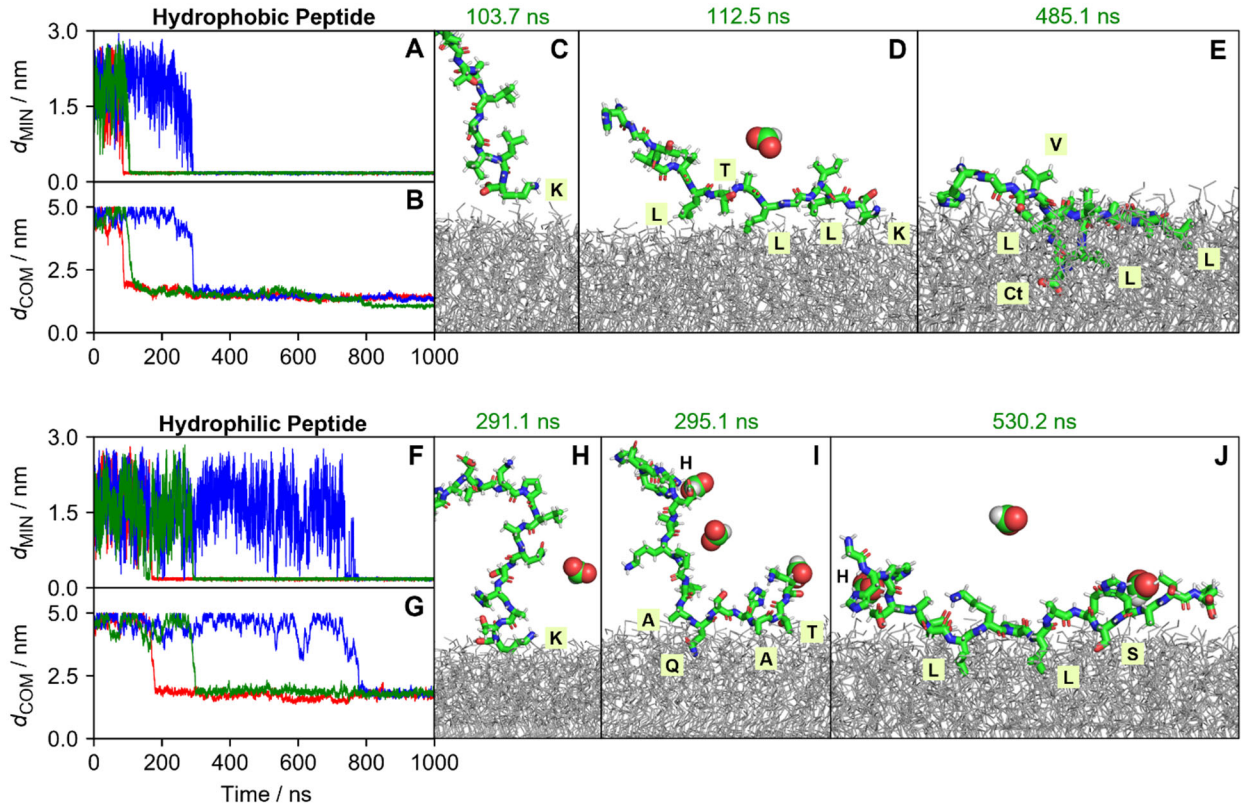

Figure 3. MD simulations of peptide trapping on the stationary phase in water. C18 chains are shown as grey lines, peptides as sticks, and formate as spheres. Solvent has been omitted for clarity. Top row: hydrophobic peptide T6. Single letter residue codes with yellow background denote residues in contact with C18 chains. (A) d_{MIN}, minimum distance between any peptide atom and the closest C18 atom. (B) d_{COM}, distance between peptide center-of-mass and the closest Si atom. Panels A/B show three independent runs in different color. (C-E) MD snapshots depicting different time points of the "green" trajectory. (F-J) Same as above, but for the hydrophilic peptide T7.

Subsequent quasi-irreversible peptide trapping encompassed burial of several side chains into the upper third of the C18 layer. Nonpolar side chains (Leu/Ile/Val) penetrated into the stationary phase most deeply, whereas charged side chains and much of the peptide backbone retained partial contact with water (Figure 3D/E, I/J). However, the trapped peptides remained very dynamic, allowing some of the nonpolar side chains to transiently protrude into the aqueous phase (Val in Figure 3E), as well as polar groups into the C18 layer (Ct in Figure 3E). The overall penetration of the trapped hydrophobic peptide into the C18 layer was somewhat deeper than for the hydrophilic peptide, with d_{COM} values of 1.5 ± 0.3 nm and 1.7 ± 0.1 nm, respectively.

Peptide Desorption. After trapping in water (Figure 3), we examined peptide desorption in water/acetonitrile. Ideally, desorption simulations would explore a range of solvent mixtures with increasing acetonitrile content, mimicking the linear gradient used for the experiments of Figure 1. However, the large computational cost of such simulations prompted us to examine just a single mixture. As noted earlier, we chose an acetonitrile content of 50/50 (mol/mol), which corresponds to 74% acetonitrile by volume. This composition was chosen because none of the myoglobin peptides were retained under these conditions (Figure 1). Six repeat simulations were conducted for each peptide. Representative data are depicted in Figure 4. All runs resulted in peptide desorption from the stationary phase within < 50 ns. For quantifying these desorption events we tracked how long it took for d_{MIN} to exceed 0.5 nm (Figure 4A/F). The desorption time points determined in this way were 13 ± 9 ns for the hydrophobic peptide T6, and 4 ± 0.7 ns for the hydrophilic peptide T7. Similar to the trapping kinetics of Figure 3, these desorption data followed the expected trend where T6 desorbed more slowly because of its higher C18 affinity.

The MD snapshots of Figure 4 illustrate different time points of the desorption process. The initial configurations represent the trapped states produced in water, where the peptides were anchored in the C18 layer, predominantly via their nonpolar residues (Figure 4C/H). Desorption in water/acetonitrile proceeded in a stepwise fashion. Initially, charged and hydrophilic moieties close to the termini lifted off into the mobile phase, while hydrophobic side chains (Leu/Ile/Val, occasionally also Ala) remained in contact with the C18 chains (Figure 4D/I). Eventually, these nonpolar contacts dissociated as well, generating free peptides in solution (Figure 4E).

It is interesting to examine the peptide solvation in water/acetonitrile during desorption. As discussed above (Figure 3), the trapped peptides were initially anchored in the C18 layer. The anchoring was primarily mediated by nonpolar side chains, while charged moieties (Nt^+, His^+,

Lys^{+}) protruded into the solvent. When exposed to water/acetonitrile, these protruding charges became extensively solvated by H_2O (Figure S4A/C). This solvation caused local enrichment of water at the sites of peptide binding, in contrast to other regions in the vicinity of the C18 chains that exhibited water depletion (Figure 2C/D). As noted, acetonitrile/water contains a network of water clusters in an acetonitrile matrix (Figure 2C). After desorption, the free peptides in this binary solvent tended to have their charged sites (particularly the termini) in contact with these water clusters (Figure S4B/D).

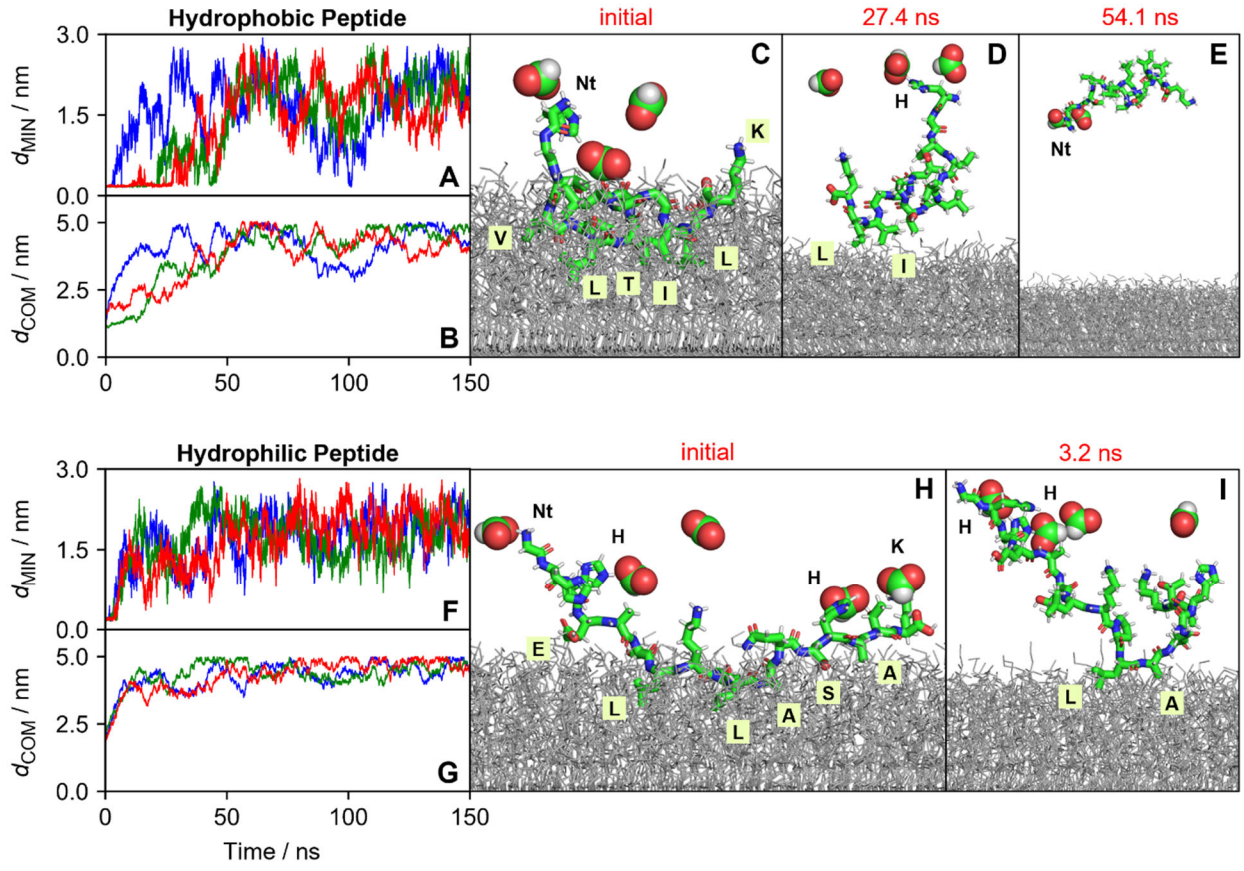

Figure 4. MD simulations of peptide desorption from the stationary phase in water/acetonitrile, after initial trapping in water. The distance metrics and graphic representations correspond to those of Figure 3. (A-E) Hydrophobic peptide T6. (F-I) Hydrophilic peptide T7. Panels A/B and F/G show three independent runs for each peptide in different color. MD snapshots in panels C-E and H/I represent different time points of the "red" trajectories.

The data discussed thus far reveal that the different hydrophobicity of the two peptides translates into different trapping and desorption kinetics. Because of its more nonpolar character, T6 exhibited faster trapping and slower desorption than T7 (Figures 3/4). Ultimately, however, trapping and desorption went to completion for both peptides within less than 1 μs, i.e., on a time scale much shorter than the elution process (Figure 1). This implies that the MD results discussed thus far cannot directly explain the differential elution of the two peptides. To uncover the reasons underlying the retention differences between T6 and T7, the subsequent section takes a closer look at the peptide behavior under elution conditions.

Differential Peptide Retention During Elution. During RPLC elution, the mobile phase flow drags analytes through the column. In the absence of analyte interactions with the stationary phase the analyte velocity would be identical to the solvent velocity. Separation relies on the fact that the analyte migration velocity is modulated by the analyte affinity to the stationary phase. Transient binding to C18 chains will temporarily anchor an analyte to the stationary phase, thereby lowering its migration velocity.[3, 13, 77] The current section examines peptide-C18 interactions that are responsible for differential peptide migration velocities in water/acetonitrile.

Three 1 μs runs were performed for each peptide. These "elution simulations" started with peptides that were positioned in the pore center. For both peptides, d_{COM} remained above ~2.5 nm, implying that most peptide atoms stayed quite far from the C18 chains during elution (Figure 5B/F). This behavior is different from trapping in water, where d_{COM} rapidly dropped to < 2 nm (Figure 3). Importantly, the elution simulations showed major differences in the d_{MIN} behavior of the two peptides. For the hydrophobic peptide T6 there were multiple incidents where d_{MIN} dipped below the 0.25 min threshold, as a result of transient peptide binding to C18 chains (Figure 5A).

All these retentive interactions were mediated by hydrophobic side chains of Val, Leu, and Ile (Figure 5C/D). In contrast, the hydrophilic peptide T7 remained well separated from the stationary phase throughout the entire simulation time with $d_{MIN} > 0.25$ (Figure 5E/G), except for a single brief interaction (Figure 5E/H). In contrast to the trapping simulations of Figure 3, C18/Lys interactions were not prevalent during elution (Figure 5).

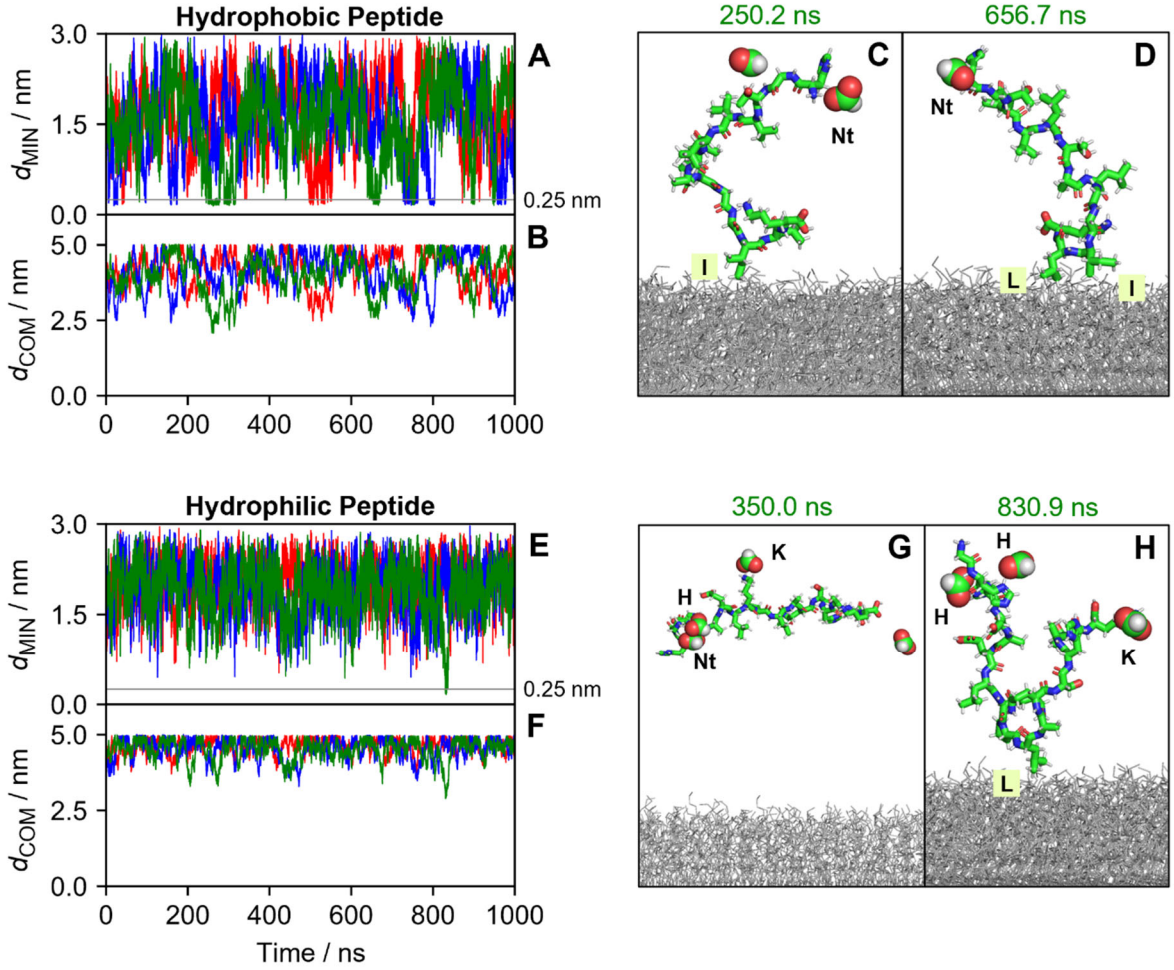

Figure 5. MD simulations of differential peptide retention during elution in water/acetonitrile. (A-D) Hydrophobic peptide T6. (E-H) Hydrophilic peptide T7. Distance metrics and graphic representations are identical to those of Figures 3 and 4. Panels A/B and E/F show three independent runs for each peptide in different color. MD snapshots in panels C/D and G/H represent different time points of the "green" trajectories.

Because our simulations did not explicitly consider mobile phase flow, the extent of peptide-C18 binding was used as a qualitative proxy for the retention behavior. We calculated the parameter f_B which represents the *f*raction of time that a peptide was *b*ound to the stationary phase. This parameter was determined by tracking d_{MIN} in 50 ps intervals. Time points with $d_{MIN} < 0.25$ nm were counted as "bound", with at least one peptide atom was in van der Waals contact with a C18 chain. Conversely, time points where $d_{MIN} > 0.25$ nm were counted as "unbound", meaning that the peptide did not interact with the stationary phase, such that f_B = (*time bound*)/(*total time*). For $f_B = 1$ a peptide would be permanently trapped on the column, whereas $f_B = 0$ would correspond to no retention.[14] For the hydrophobic peptide T6, the elution simulations of Figure 5 correspond to $f_B = 0.034$. In contrast, the hydrophilic peptide T7 had $f_B = 0.001$. These MD-derived f_B values qualitatively match the experimentally observed trend, where T6 was retained more strongly than T7 (Figure 1). Overall, it is remarkable that our MD strategy correctly captures key aspects of the RPLC process, although the absence of a solvent gradient precludes using the Figure 5 data for quantitative retention predictions.

Ion Pairing. RPLC separations generally involve an ion pairing agent that can bind to analytes via electrostatic (cation-anion) contacts, thereby enhancing the retention of polar species. The basic properties of various ion pairing agents have been studied experimentally, but many molecular details remain to be uncovered.[7-12] One key question is how the extent of ion pairing depends on the mobile phase composition. The data of this work provide insights into the behavior of formate which represents the most common ion pairing agent for peptide RPLC.[1, 8]

Ion pairing during our RPLC simulations was tracked by monitoring peptide-formate distances for all atoms. For distances below a certain cut-off, the corresponding amino acid was considered to be ion-paired. N- and C-termini were treated separately from the corresponding

amino acids. The analysis was conducted with two cutoff values: 0.25 nm was used to probe direct van der Waals contacts. A larger cutoff of 0.5 nm served to additionally capture instances where formate resided in the vicinity of a charged site, but not directly bound to it (i.e., in loose "screening contact" with the peptide).[38] None of the ion pairing contacts were permanent; instead, peptide-formate association/dissociation events took place within tens of nanoseconds (Figure S5). The MD data were compiled into f_{IP} values which represent the *f*raction of time that any peptide moiety was *i*on *p*aired. A value of $f_{IP} = 1$ would indicate that a residue is engaged in ion pairing all the time, whereas $f_{IP} = 0$ represents the absence of ion pairing. Figure 6 reveals that the overall extent of ion pairing was larger for T7 than for T6, reflecting the higher positive charge of the hydrophilic peptide (6+ vs. 3+). The f_{IP} data of Figure 6 reveal additional interesting features:

(i) As expected, formate-peptide interactions were found predominantly at cationic sites, i.e., N-termini and His/Lys side chains. The four N-terminal residues showed the highest ion pairing propensity, reflecting the accumulation of cationic sites in these regions (two positive charges for T6, and three positive charges for T7). Such N-terminal ion pairing has previously been suggested to play an important role for the peptide retention behavior.[38]

(ii) Ion pairing was less pronounced in water than in water/acetonitrile, evident from the fact that the f_{IP} values in Figure 6A/B are lower than the corresponding values in Figure 6C/D. This trend can be attributed to the fact that H_2O weakens cation/anion interactions by outcompeting them via ion/dipole binding, and by increasing the dielectric constant.[43] Both factors are less pronounced in the presence of acetonitrile, a molecule with lower H-bonding propensity and a weaker dipole moment.[72] Hence, our data reveal that the capability of formate to lower the peptide hydrophilicity via cation/anion binding[7-12] is markedly more pronounced in water/acetonitrile than

in water. We conclude that ion pairing with formate is unlikely to play a major role during peptide trapping, where the mobile phase is mostly aqueous (Figure 3).

(iii) The overall patterns for both cutoff values are quite similar, with 1 > f_{IP}(0.5 nm) > f_{IP}(0.25 nm). This implies that even in the absence of direct contacts, formate tends to remain in the vicinity of cationic sites on the peptide.

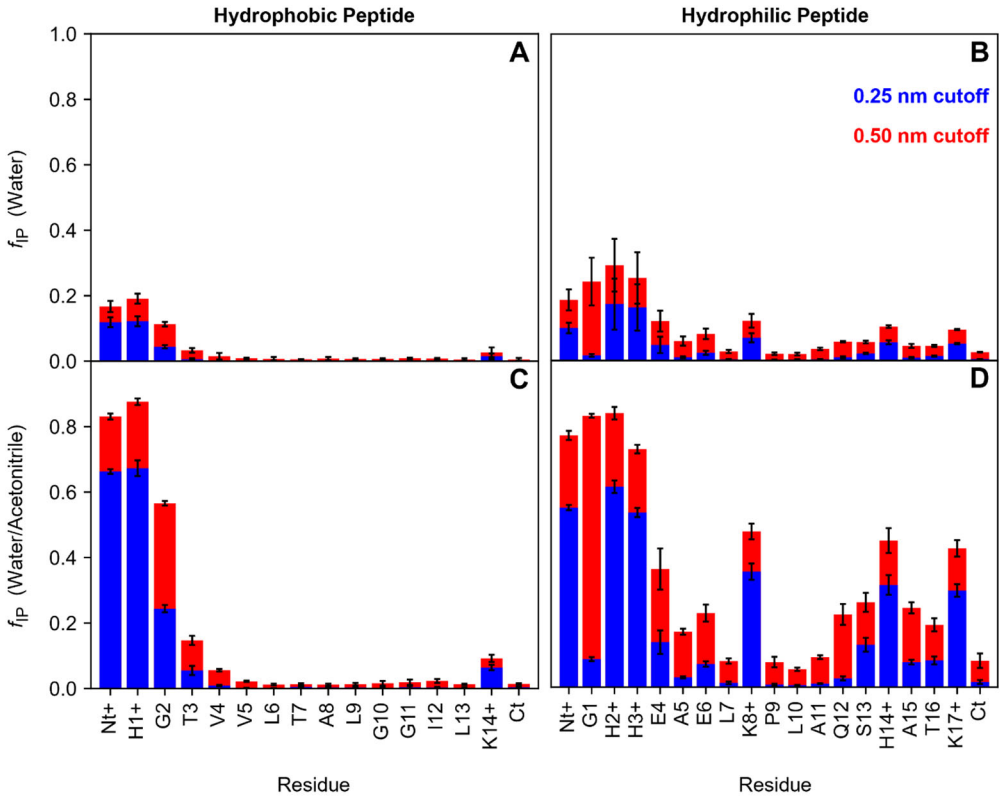

Figure 6. Extent of ion pairing during peptide trapping in water (A, B) and during elution in acetonitrile/water (C, D). Panels A/C: hydrophobic peptide T6; panels B/D: hydrophilic peptide T7. The *y*-axes represent f_{IP}, i.e., the fraction of time that peptide moieties (listed along the *x*-axes) were paired with a formate ion. f_{IP} values were calculated for distance cutoffs of 0.25 nm (blue) and 0.5 nm (red). These data were derived from the trajectories of Figures 3 and 5, sampled in 0.05 ns intervals. Error bars represent standard deviations.

Conclusions

Despite the widespread use of RPLC, most existing workflows were developed using empirical trial and error strategies. Atomistic details of the interactions between stationary phase, mobile phase, and analytes have remained poorly understood for many years. The current study provides an in-depth molecular view of peptide RPLC using MD simulations. Standard MD force fields of the type employed here were designed primarily to model protein folding and dynamics in water.[60] It is a testament to the robustness of these force fields that they can also be applied to peptide/stationary phase interactions in mixed solvents. To the best of our knowledge, this work marks the first time that MD simulations successfully captured all stages of peptide RPLC, i.e., trapping on C18 chains in water, as well as desorption, and differential elution in water/acetonitrile.

One of the key questions that has been discussed in the RPLC literature is whether analytes interact with the stationary phase via adsorption, or whether they partition into the stationary phase.[16-20] Our peptide simulations exhibit elements of both scenarios. In contrast to small hydrocarbons,[19, 53-56] the sheer size of tryptic peptides precludes them from completely partitioning into the C18 stationary phase. Nonetheless, certain parts of the peptides (the hydrophobic side chains of Leu/Ile/Val) were found to penetrate quite deep into the C18 layer during peptide trapping in water, reminiscent of a partitioning process. In contrast, peptide elution in water/acetonitrile proceeded with adsorption-like behavior, characterized by transient binding of Leu/Ile/Val side chains to C18 chains at the stationary/mobile phase interface. Peptide-C18 association and dissociation were readily observable on the 1 μs time scale of our MD runs, whereas many of these dynamic events would have gone undetected in the much shorter time windows used for earlier RPLC simulations.[57, 58]

Our work sets the stage for future MD simulations that will be able to assist in the development of improved retention prediction algorithms. We also envision that MD simulations will become helpful for the design of novel column materials and ion pairing agents that are tailored for specific applications. The computational cost of such endeavors may be quite high, but we are confident that ongoing improvements of computer hardware and software will help overcome existing hurdles in a few years' time. In any case, the success of the current work raises the possibility that MD simulations will one day become an integral part of the chromatographer's tool box.

Acknowledgments. We thank Oleg Krokhin and Darien Yeung for helpful discussions. Funding for this work was provided by the Natural Sciences and Engineering Research Council of Canada (RGPIN-2018-04243).

Supporting Information. Complete Methods Section. Figure S1: Layout of stationary phase. Figure S2: Plot of elution time vs. KD hydropathy. Figure S3: MD snapshots of solvent craters in the C18 layer. Figure S4: MD snapshots of peptide solvation during and after desorption. Figure S5: Ion pairing dynamics in water/acetonitrile.

References

(1) D'Atri, V.; Murisier, A.; Fekete, S.; Veuthey, J. L.; Guillarme, D. Current and future trends in reversed-phase liquid chromatography-mass spectrometry of therapeutic proteins. *Trac-Trends Anal. Chem.* **2020**, 130, 9.
(2) Žuvela, P.; Skoczylas, M.; Jay L., J.; Bączek, T.; Kaliszan, R.; Wong, M. W.; Buszewski, B. Column Characterization and Selection Systems in Reversed-Phase High-Performance Liquid Chromatography. *Chem. Rev.* **2019**, 119, 3674-3729.
(3) Heftmann, E. *Chromatography*; Elsevier: Amsterdam, 2004.

(4) Claessens, H. A.; van Straten, M. A. Review on the chemical and thermal stability of stationary phases for reversed-phase liquid chromatography. *J. Chromatogr. A* **2004**, 1060, 23-41.
(5) Fekete, S.; Veuthey, J. L.; Guillarme, D. New trends in reversed-phase liquid chromatographic separations of therapeutic peptides and proteins: Theory and applications. *J. Pharm. Biomed. Anal.* **2012**, 69, 9-27.
(6) Bell, D. S.; Green, A. I.; Lopez, D. A. Columns - What is on Your HPLC Particle? A Look at Stationary Phase Chemistry Synthesis. *LCGC Asia Pacific* **2021**, 24, 28-33.
(7) Cecchi, T. Ion pairing chromatography. *Crit. Rev. Anal. Chem.* **2008**, 38, 161-213.
(8) Gussakovsky, D.; Anderson, G.; Spicer, V.; Krokhin, O. V. Peptide separation selectivity in proteomics LC-MS experiments: Comparison of formic and mixed formic/heptafluorobutyric acids ion-pairing modifiers. *J. Sep. Sci.* **2020**, 43, 3830-3839.
(9) Horvath, C.; Melander, W.; Molnar, I.; Molnar, P. Enhancement of Retention by Ion-Pair Formation in Liquid Chromatography with Nonpolar Stationary Phases. *Anal. Chem.* **1977**, 49, 2295-2305.
(10) Nguyen, J. M.; Smith, J.; Rzewuski, S.; Legido-Quigley, C.; Lauber, M. A. High sensitivity LC-MS profiling of antibody-drug conjugates with difluoroacetic acid ion pairing. *mAbs* **2019**, 11, 1358-1366.
(11) Sagi-Kiss, V.; Li, Y.; Carey, M. R.; Grover, S. J.; Siems, K.; Cirulli, F.; Berry, A. H.; Musillo, C.; Wilson, I. D.; Want, E. J.; Bundy, J. G. Ion-Pairing Chromatography and Amine Derivatization Provide Complementary Approaches for the Targeted LC-MS Analysis of the Polar Metabolome. *J. Proteome Res.* **2022**, 21, 1428−1437.
(12) Garcia, M. C. The effect of the mobile phase additives on sensitivity in the analysis of peptides and proteins by high-performance liquid chromatography-electrospray mass spectrometry. *J. Chromatogr. B* **2005**, 825, 111-123.
(13) Lenčo, J.; Jadeja, S.; Naplekov, D. K.; Krokhin, O. V.; Khalikova, M. A.; Chocholouš, P.; Urban, J.; Broeckhoven, K.; Nováková, L.; Švec, F. Reversed-Phase Liquid Chromatography of Peptides for Bottom-Up Proteomics: A Tutorial. *J. Proteome Res.* **2022**, 21, 2846–2892.
(14) Scott, R. P. W. Modern liquid chromatography. *Chem. Soc. Rev.* **1992**, 21, 137-145.
(15) Moruz, L.; Kall, L. Peptide Retention Time Prediction. *Mass Spectrom. Rev.* **2017**, 36, 615-623.
(16) Berek, D. Progress in Liquid Chromatography of Synthetic Electroneutral Polymers. *Macromol. Symp.* **2003**, 195, 147-164.
(17) Vailaya, A.; Horvath, C. Retention in reversed-phase chromatography: partition or adsorption? *J. Chromatogr. A* **1998**, 829, 1-27.
(18) Kaczmarski, K.; Prus, W.; Kowalska, T. Adsorption/partition model of liquid chromatography for chemically bonded stationary phases of the aliphatic cyano, reversed-phase C8 and reversed-phase C18 types. *J. Chromatogr. A* **2000**, 869, 57-64.
(19) Rafferty, J. L.; Siepmann, J. I.; Schure, M. R. Mobile phase effects in reversed-phase liquid chromatography: A comparison of acetonitrile/water and methanol/water solvents as studied by molecular simulation. *J. Chromatogr. A* **2011**, 1218, 2203-2213.
(20) Mabry, J. N.; Skaug, M. J.; Schwartz, D. K. Single-Molecule Insights into Retention at a Reversed-Phase Chromatographic Interface. *Anal. Chem.* **2014**, 86, 9451-9458.
(21) Cech, N. B.; Enke, C. G. Practical Implication of Some Recent Studies in Electrospray Ionization Fundamentals. *Mass Spectrom. Rev.* **2001**, 20, 362-387.

(22) Thomson, B. A. Atmospheric Pressure Ionization and Liquid Chromatography/Mass Spectrometry-Together at Last. *J. Am. Soc. Mass Spectrom.* **1998**, 9, 187-193.
(23) Apffel, A.; Fischer, S.; Goldberg, G.; Goodley, P. C.; Kuhlmann, F. E. Enhanced sensitivity for peptide mapping with electrospray liquid chromatography-mass spectrometry in the presence of signal suppression due to trifluoroacetic acid-containing mobile phases. *J. Chromatogr. A* **1995**, 712, 177-190.
(24) Rodriguez, J.; Gupta, N.; Smith, R. D.; Pevzner, P. A. Does Trypsin Cut Before Proline? *J. Proteome Res.* **2008**, 7, 300-305.
(25) Zhang, Y.; Fonslow, B. R.; Shan, B.; Baek, M.-C.; Yates, J. R. Protein Analysis by Shotgun/Bottom-up Proteomics. *Chem. Rev.* **2013**, 113, 2343-2394.
(26) Olsen, J. V.; Ong, S.; Mann, M. Trypsin Cleaves Exlusively C-terminal to Arginine and Lysine Residues. *Mol. Cell. Proteomics* **2004**, 3, 608-614.
(27) Masson, G. R.; Burke, J. E.; Ahn, N. G.; Anand, G. S.; Borchers, C. H.; Brier, S.; Bou-Assaf, G. M.; Engen, J. R.; Englander, S. W.; Faber, J. H.; Garlish, R. A.; Griffin, P. R.; Gross, M. L., et al. Recommendations for performing, interpreting and reporting hydrogen deuterium exchange mass spectrometry (HDX-MS) experiments. *Nat. Methods* **2019**, 16, 595-602.
(28) Ziemianowicz, D. S.; MacCallum, J. L.; Schriemer, D. C. Correlation between Labeling Yield and Surface Accessibility in Covalent Labeling Mass Spectrometry. *J. Am. Soc. Mass Spectrom.* **2020**, 31, 207-216.
(29) Sharp, J. S.; Chea, E. E.; Misra, S. K.; Orlando, R.; Popov, M.; Egan, R. W.; Holman, D.; Weinberger, S. R. Flash Oxidation (FOX) System: A Novel Laser-Free Fast Photochemical Oxidation Protein Footprinting Platform. *J. Am. Soc. Mass Spectrom.* **2021**, 32, 1601-1609.
(30) Leitner, A.; Bonvin, A.; Borchers, C. H.; Chalkley, R. J.; Chamot-Rooke, J.; Combe, C. W.; Cox, J.; Dong, M. Q.; Fischer, L.; Gotze, M.; Gozzo, F. C.; Heck, A. J. R.; Hoopmann, M. R., et al. Toward Increased Reliability, Transparency, and Accessibility in Cross-linking Mass Spectrometry. *Structure* **2020**, 28, 1259-1268.
(31) Piersimoni, L.; Kastritis, P. L.; Arlt, C.; Sinz, A. Cross-Linking Mass Spectrometry for Investigating Protein Conformations and Protein – Protein Interactions—A Method for All Seasons. *Chem. Rev.* **2022**, 122, 7500-7531.
(32) Gillet, L. C.; Leitner, A.; Aebersold, R. Mass Spectrometry Applied to Bottom-Up Proteomics: Entering the High-Throughput Era for Hypothesis Testing. *Annu. Rev. Anal. Chem.* **2016**, 9, 449-472.
(33) Creighton, T. E. *Proteins*; W. H. Freeman & Co: New York, 1993.
(34) Dillon, T. M.; Bondarenko, P. V.; Rehder, D. S.; Pipes, G. D.; Kleemann, G. R.; Ricci, M. S. Optimization of a reversed-phase high-performance liquid chromatography/mass spectrometry method for characterizing recombinant antibody heterogeneity and stability. *J. Chromatogr. A* **2006**, 1120, 112-120.
(35) Tome, T.; Žigart, N.; Časar, Z.; Obreza, A. Development and Optimization of Liquid Chromatography Analytical Methods by Using AQbD Principles: Overview and Recent Advances. *Org. Process Res. Dev.* **2019**, 23, 1784-1802.
(36) Perez de Souza, L.; Alseekh, S.; Scossa, F.; Fernie, A. R. Ultra-high-performance liquid chromatography high-resolution mass spectrometry variants for metabolomics research. *Nat. Methods* **2021**, 18, 733-746.
(37) Haddad, P. R.; Taraji, M.; Szücs, R. Prediction of Analyte Retention Time in Liquid Chromatography. *Anal. Chem.* **2021**, 93, 228-256.

(38) Krokhin, O. V.; Craig, R.; Spicer, V.; Ens, W.; Standing, K. G.; Beavis, R. C.; Wilkins, J. A. An improved model for prediction of retention times of tryptic peptides in ion pair reversed-phase HPLC - Its application to protein peptide mapping by off-line HPLC-MALDI MS. *Mol. Cell. Proteomics* **2004**, 3, 908-919.
(39) Spicer, V.; Yamchuk, A.; Cortens, J.; Sousa, S.; Ens, W.; Standing, K. G.; Wilkins, J. A.; Krokhin, O. V. Sequence-Specific Retention Calculator. A Family of Peptide Retention Time Prediction Algorithms in Reversed-Phase HPLC: Applicability to Various Chromatographic Conditions and Columns. *Anal. Chem.* **2007**, 79, 8762-8768.
(40) Ma, C.; Ren, Y.; Yang, J.; Ren, Z.; Yang, H.; Liu, S. Improved Peptide Retention Time Prediction in Liquid Chromatography through Deep Learning. *Anal. Chem.* **2018**, 90, 10881-10888.
(41) Gritti, F. Perspective on the Future Approaches to Predict Retention in Liquid Chromatography. *Anal. Chem.* **2021**, 93, 5653-5664.
(42) Shaw, D. E.; Maragakis, P.; Lindorff-Larsen, K.; Piana, S.; Dror, R. O.; Eastwood, M. P.; Bank, J. A.; Jumper, J. M.; Salmon, J. K.; Shan, Y.; Wriggers, W. Atomic Level Characterization of the Structural Dynamics of Proteins. *Science* **2010**, 330, 341-346.
(43) Brini, E.; Fennell, C. J.; Fernandez-Serra, M.; Hribar-Lee, B.; Luksic, M.; Dill, K. A. How Water's Properties Are Encoded in Its Molecular Structure and Energies. *Chem. Rev.* **2017**, 117, 12385-12414.
(44) Aliyari, E.; Konermann, L. Formation of Gaseous Peptide Ions from Electrospray Droplets: Competition between the Ion Evaporation Mechanism and Charged Residue Mechanism. *Anal. Chem.* **2022**, 94, 7713-7721.
(45) Lindsey, R. K.; Rafferty, J. L.; Eggimann, B. L.; Siepmann, J. I.; Schure, M. R. Molecular simulation studies of reversed-phase liquid chromatography. *J. Chromatogr. A* **2013**, 1287, 60-82.
(46) Melnikov, S. M.; Höltzel, A.; Seidel-Morgenstern, A.; Tallarek, U. A Molecular Dynamics View on Hydrophilic Interaction Chromatography with Polar-Bonded Phases: Properties of the Water-Rich Layer at a Silica Surface Modified with Diol-Functionalized Alkyl Chains. *J. Phys. Chem. C* **2016**, 120, 13126-13138.
(47) Zhang, L.; Sun, L.; Siepmann, J. I.; Schure, M. R. Molecular simulation study of the bonded-phase structure in reversed-phase liquid chromatography with neat aqueous solvent. *J. Chromatogr. A* **2005**, 1079, 127-135.
(48) Klatte, S. J.; Beck, T. L. Molecular Dynamics Simulations of Tethered Alkane Chromatographic Stationary Phases. *J. Phys. Chem.* **1995**, 99, 16024-16032.
(49) Rafferty, J. L.; Siepmann, J. I.; Schure, M. R. Molecular-Level Comparison of Alkylsilane and Polar-Embedded Reversed-Phase Liquid Chromatography Systems. *Anal. Chem.* **2008**, 80, 6214-6221.
(50) Lippa, K. A.; Sander, L. C.; Mountain, R. D. Molecular Dynamics Simulations of Alkylsilane Stationary-Phase Order and Disorder. 2. Effects of Temperature and Chain Length. *Anal. Chem.* **2005**, 77, 7862-7871.
(51) Mansfield, E. R.; Mansfield, D. S.; Patterson, J. E.; Knotts, T. A. Effects of Chain Grafting Positions and Surface Coverage on Conformations of Model Reversed-Phase Liquid Chromatography Stationary Phases. *J. Phys. Chem. C* **2012**, 116, 8456-8464.
(52) Gupta, P. K.; Meuwly, M. Dynamics of Water/Methanol Mixtures at Functionalized Chromatographic Interfaces. *J. Phys. Chem. B* **2012**, 116, 10951-10959.

(53) Klatte, S. J.; Beck, T. L. Microscopic Simulation of Solute Transfer in Reversed Phase Liquid Chromatography. *J. Phys. Chem.* **1996**, 100, 5931-5934.
(54) Slusher, J. T.; Mountain, R. D. A molecular dynamics study of a reversed-phase liquid chromatography model. *J. Phys. Chem. B* **1999**, 103, 1354-1362.
(55) Rybka, J.; Holtzel, A.; Steinhoff, A.; Tallarek, U. Molecular Dynamics Study of the Relation between Analyte Retention and Surface Diffusion in Reversed-Phase Liquid Chromatography. *J. Phys. Chem. C* **2019**, 123, 3672-3681.
(56) Cheng, C.-Y.; Chen, T.-L.; Wang, B.-C. Molecular dynamics simulation of separation mechanisms in bonded phase liquid chromatography. *J. Mol. Struct. THEOCHEM* **2002**, 577, 81-90.
(57) Yarovsky, I.; Hearn, M. T. W.; Aguilar, M. I. Molecular Simulation of Peptide Interactions with an RP-HPLC Sorbent. *J. Phys. Chem. B* **1997**, 101, 10962-10970.
(58) Tsai, C. W.; Chen, W. Y.; Ruaan, R. C. Retention Prediction of Peptide Diastereomers in Reversed-Phase Liquid Chromatography Assisted by Molecular Dynamics Simulation. *Langmuir* **2012**, 28, 13601-13608.
(59) Abraham, M. J.; Murtola, T.; Schulz, R.; Páll, S.; Smith, J. C.; Hess, B.; Lindahl, E. GROMACS: High performance molecular simulations through multi-level parallelism from laptops to supercomputers. *SoftwareX* **2015**, 1–2, 19-25.
(60) Huang, J.; Rauscher, S.; Nawrocki, G.; Ran, T.; Feig, M.; de Groot, B. L.; Grubmuller, H.; MacKerell, A. D. CHARMM36m: an improved force field for folded and intrinsically disordered proteins. *Nat. Methods* **2017**, 14, 71-73.
(61) Borges, E. M. Silica, Hybrid Silica, Hydride Silica and Non-Silica Stationary Phases for Liquid Chromatography. *J. Chromatogr. Sci.* **2015**, 53, 580-597.
(62) Petersson, P.; Euerby, M. R. Characterisation of RPLC columns packed with porous sub-2 mu m particles. *J. Sep. Sci.* **2007**, 30, 2012-2024.
(63) Szepesy, L. Evaluation of column characteristics in RPLC using linear solvation energy relationships (LSERs). *J. Sep. Sci.* **2003**, 26, 201-214.
(64) Rybka, J.; Höltzel, A.; Tallarek, U. Surface Diffusion of Aromatic Hydrocarbon Analytes in Reversed-Phase Liquid Chromatography. *J. Phys. Chem. C* **2017**, 121, 17907-17920.
(65) Giaquinto, A.; Liu, Z. X.; Bach, A.; Kazakevich, Y. Surface area of reversed-phase HPLC columns. *Anal. Chem.* **2008**, 80, 6358-6364.
(66) Krokhin, O. V. Sequence-Specific Retention Calculator. Algorithm for Peptide Retention Prediction in Ion-Pair RP-HPLC: Application to 300- and 100-Å Pore Size C18 Sorbents. *Anal. Chem.* **2006**, 78, 7785-7795.
(67) Kyte, J.; Doolittle, R. A simple method for displaying the hydropathic character of a protein. *J. Mol. Biol.* **1982**, 157, 105-132.
(68) Spicer, V.; Lao, Y. W.; Shamshurin, D.; Ezzati, P.; Wilkins, J. A.; Krokhin, O. V. N-Capping Motifs Promote Interaction of Amphipathic Helical Peptides with Hydrophobic Surfaces and Drastically Alter Hydrophobicity Values of Individual Amino Acids. *Anal. Chem.* **2014**, 86, 11498-11502.
(69) Liang, C.; Qiao, J. Q.; Lian, H. Z. Determination of reversed-phase high performance liquid chromatography based octanol-water partition coefficients for neutral and ionizable compounds: Methodology evaluation. *J. Chromatogr. A* **2017**, 1528, 25-34.
(70) Ganesh, V.; Basuri, P. P.; Sahini, K.; Nalini, C. N. Retention behaviour of analytes in reversed-phase high-performance liquid chromatography-A review. *Biomed. Chromatogr.* **2022**, e5482.

(71) Regnier, F. E. The Role of Protein Structure in Chromatographic Behavior. *Science* **1987**, 238, 319-323.
(72) Mountain, R. D. Microstructure and Hydrogen Bonding in Water−Acetonitrile Mixtures. *J. Phys. Chem. B* **2010**, 114, 16460-16464.
(73) Guo, J. H.; Luo, Y.; Augustsson, A.; Kashtanov, S.; Rubensson, J. E.; Shuh, D. K.; Agren, H.; Nordgren, J. Molecular structure of alcohol-water mixtures. *Phys. Rev. Lett.* **2003**, 91, 157401.
(74) Dixit, S.; Crain, J.; Poon, W. C. K.; Finney, J. L.; Soper, A. K. Molecular segregation observed in a concentrated alcohol-water solution. *Nature* **2002**, 416, 829-832.
(75) Allison, S. K.; Fox, J. P.; Hargreaves, R.; Bates, S. P. Clustering and microimmiscibility in alcohol-water mixtures: Evidence from molecular-dynamics simulations. *Phys. Rev. B* **2005**, 71, 024201.
(76) Ng, Y. K.; Tajoddin, N. N.; Scrosati, P. M.; Konermann, L. Mechanism of Thermal Protein Aggregation: Experiments and Molecular Dynamics Simulations on the High-Temperature Behavior of Myoglobin. *J. Phys. Chem. B* **2021**, 125, 13099-13110.
(77) Yamamoto, S.; Nomura, M.; Sano, Y. Adsorption chromatography of proteins: Determination of optimum conditions. *AIChE J.* **1987**, 33, 1426-1434.

For Table of Contents Only